*Acta Cryst.* (1999). A**55**, 500–507

# The use of multiple-scattering data to enhance small-angle neutron scattering experiments

T. M. Sabine* and W. K. Bertram

*Materials Division, ANSTO, Menai, NSW 2234, Australia. E-mail: tms@ansto.gov.au*

(*Received 13 February 1998; accepted 16 October 1998*)

## Abstract

Multiple scattering of neutrons by the inhomogeneities responsible for small-angle neutron scattering (SANS) during the passage of the beam through the specimen can be used to provide valuable information about the shape of the objects and the absolute value of the contrast between the scattering particles and the matrix. The neutrons emerging from the specimen are classified into those that have been scattered $n$ times. The index $n$ ranges from zero to infinity. The remnant of the incident beam is the group of neutrons for which $n$ equals zero. Each group contributes separately to the scattering profile. The small-angle scattering cross section is independent of the neutron wavelength for $n = 1$ only. Thus collection of data as a function of specimen thickness and of neutron wavelength will provide a number of different profiles describing the same physical situation. Simultaneous analysis of these profiles provides absolute values of the cross section for scattering into the small-angle region and of the cross section for removal of neutrons from the small-angle region. So that the method can be used generally, a profile function that is a very good approximation to those in the literature is introduced. The implications for time-of-flight SANS are discussed.

## 1. Introduction

The technique of small-angle scattering involves the experimental investigation of the strong maximum in the scattered intensity at a scattering angle close to zero. When the coherent scattering cross section of the nuclei in the specimen is nonzero, this reflection will always exist whatever the state of spatial order in the specimen. It corresponds to the zeroth-order spectrum from a crystal lattice (James, 1948).

It will be assumed in this analysis that no long-range order exists in the inhomogeneities under investigation or in the matrix in which they are immersed. This is almost always the case in small-angle scattering experiments.

In a SANS experiment, the profile of the (0, 0, 0) reflection is measured as a function of the scattering angle after the incident beam has passed through the specimen. In the usual SANS data-analysis procedure, two assumptions are made. The first is that the incident beam is not depleted in the experiment. This leads to the simple method of obtaining the SANS scattering by subtraction of the pattern obtained in an identical experiment without the specimen (Agamalian *et al.*, 1997). The second assumption is that of single scattering. Both these assumptions will always hold for a sufficiently thin specimen or sufficient degree of dilution of the entities giving rise to SANS. However, in many cases in materials science, the degree of dilution is controlled by the chemistry of the material, and grinding or polishing to reduce the physical thickness may produce a specimen that is not representative of the bulk material. An additional complication is the necessary superposition of the incident beam on a much less intense small-angle scattering profile. In practice, this means that the small-angle profile can only be seen as wings on the dominant incident beam. The result is uncertainty in the interpretation, as the region at low momentum transfer (the Guinier region) is not accessible to the experimenter.

In this work, a very different approach is proposed. The neutrons that emerge from the specimen are classified according to the number of times, $n$, they have been scattered during their passage through the specimen. The values of $n$ range from zero to infinity. The remnant of the incident beam is that component for which $n = 0$. Depletion of the incident beam during its passage through the specimen is taken into account.

It will be shown that SANS patterns from specimens that are of different thickness, but are otherwise identical, not only provide information on the shape and size of the scattering entity but also provide absolute values of the scattering contrast between the particles responsible for SANS and the matrix. No separate calibration of the incident beam is required. The methods used are similar to those of Warren (1949), Dexter & Beeman (1949) and Schelten & Schmatz (1980). The new feature is the explicit inclusion of the incident beam as a component of the scattering profile.

In the present approach, only interparticle scattering (which is the analogue of secondary extinction in conventional crystallography) is considered to be operative. Weiss (1951) has shown that the criterion for the use of kinematic diffraction theory is the condition that the neutron phase shift in traversing a particle is not

Table 1. *Definition of symbols*

| | |
|---|---|
| $\Phi_0$ | Flux of the incident beam (neutrons $cm^{-2}\ s^{-1}$). |
| $R$ | Radius of the particle |
| $V_p$ | Volume of the particle |
| $N_m$ | Number of molecules per unit volume in the particle |
| $N_o$ | Number of molecules per unit volume in the matrix |
| $b_m$ | Coherent scattering length per particle molecule |
| $b_o$ | Coherent scattering length per matrix molecule |
| $\lambda$ | Wavelength of the incident radiation |
| $\theta$ | Angle between the incident and scattered beams |
| $q$ | $4\pi \sin(\theta/2)/\lambda$ |
| $I_0$ | Differential cross section per unit volume for scattering into the small-angle region at $q = 0$ |
| $\sigma$ | Total scattering cross section per unit volume for scattering into the small-angle region |
| $\mu$ | Total scattering cross section for removal of neutrons from the small-angle region, both by scattering and by absorption |
| $\tau$ | Total cross section for depletion of the incident beam $(= \sigma + \mu)$ |
| $\sigma_s$, $\sigma_a$ | Conventional scattering and absorption cross sections, respectively, per molecule |
| $t$ | Thickness of specimen |
| $f$ | Volume fraction of particles in the specimen |

significantly different from the phase shift in travelling the same distance in a vacuum. This condition is similar to the criterion for primary extinction in conventional crystallography (Sabine, 1992) and, in general, kinematic theory is adequate for particles less than 1 μm in size; that is to say that multiple scattering *within* a particle of this size can be neglected.

As the thickness of the specimen increases so does the likelihood that the incident neutron is scattered more than once. Multiple scattering occurs when the scattered rays from particles in the layers nearest the incident surface act as the incident beams for particles in subsequent layers. In the electron diffraction literature (Cowley, 1981), this type of scattering is called incoherent multiple scattering since there is no phase relationship between different scattering centres. In neutron diffraction, incoherent scattering has a well established and different meaning. The term multiple scattering will be used in this work. The physical result is a broadening of the profile of the scattered radiation, which, if not properly taken into account, leads to an underestimate of the size of the scattering particle. It has been suggested by Mazumder & Sequira (1989) that this feature could be used to study large particles from which the scattering would, under single-scattering conditions, fall within the incident beam.

The Rietveld method (Rietveld, 1969) is used extensively to refine the parameters that contribute to the intensities of Bragg reflections in neutron and X-ray powder patterns. The philosophy of the method is the formulation of an expected intensity distribution, $I^{\rm calc}$, from approximate values of the parameters, and the least-squares refinement of $I^{\rm calc}$ against the observed intensity distribution, $I^{\rm obs}$. The variables in the refinement are the values of the parameters. A similar approach can be applied to the analysis of SANS data.

The implication of the wavelength dependence of multiple scattering in time-of-flight SANS experiments is discussed qualitatively.

## 2. Definition of terms

The objective of the experiment is the determination of the shape, size and composition of the scattering particles, which are agglomerates of molecules, embedded in a matrix with different scattering properties. By analogy with the unit cell of a crystal, the basic structural unit in this work is taken to be the molecule. As a result, the coherent scattering length per molecule corresponds to the conventional $F(0)$ of crystallography. The symbols used in this work are defined in Table 1.

## 3. Kinematic theory

Within the kinematic theory, the basic equation for the total intensity of coherent scattering by an assemblage of nuclei is

$$I(q) = \sum_{j=0}^{N-1} \sum_{j'=0}^{N-1} b_j b_{j'}^* \exp[i\mathbf{q} \cdot (\mathbf{r}_j - \mathbf{r}_{j'})]. \qquad (1)$$

The coherent scattering length is $b_j$. The sum is over all nuclei ($N$) in the irradiated volume, and $I(q)$, which is equal to the coherent differential cross section, is the scattered intensity per unit incident flux. This equation can be written for an assemblage of nuclei of scattering length $b$ (which is assumed to be real) as

$$I(q) = b^2 \left\{ N + \sum^{N-1} \sum_{j' \neq j}^{N-1} \exp[i\mathbf{q} \cdot (\mathbf{r}_j - \mathbf{r}_{j'})] \right\}. \qquad (2)$$

In an exact analysis of the scattering by a spherical particle of radius $R$ containing $N$ nuclei with scattering length $b$ and a random spatial arrangement, James (1948) has shown that this expression becomes

$$I(q) = b^2[N + N(N-1)F(q)^2], \qquad (3)$$

where $F(q)$ is the form factor given by

$$F(q) = 3[\sin(qR) - qR\cos(qR)]/(qR)^3. \qquad (4)$$

Since $N$ is large, $N(N-1)$ can be replaced by $N^2$ in the second term of (3) without significant error in this term. This leads to the standard expression per particle for scattering into the small-angle region:

$$I(q) = [NbF(q)]^2. \qquad (5)$$

While the neglect of the approximation above has a negligible effect on the evaluation of the small-angle scattering, it is necessary to include the first term of equation (30) to account for the removal cross section for neutrons traversing the specimen. The statement by

May (1992) implying that the diffuse background contains only incoherent scattering is incorrect.

To generalize to a particle of $N_m$ molecules per unit volume, each with scattering length $b_m$, contained in an extended matrix with $N_o$ molecules per unit volume, each of scattering length $b_o$, the amplitude of scattering, following the method of Krivoglaz (1969), is written as

$$A(q) = \sum_{j}^{\text{all sites}} b_o \exp(i\mathbf{q}\cdot\mathbf{r}_j) + \sum_{m}^{N,m} b_m \exp(i\mathbf{q}\cdot\mathbf{r}_m) - \sum_{o}^{N,m} b_o \exp(i\mathbf{q}\cdot\mathbf{r}_o).$$

The intensity per unit volume, $A(q)A^*(q)$, for amorphous specimens is then given by

$$I(q) = f N_m b_m^2 + (1-f)N_o b_o^2 + f(N_m b_m - N_o b_o)^2 F(q)^2. \quad (6)$$

For dilute systems, interference between radiation scattered by nuclei or molecules located in different particles can be ignored, and if in addition the particles can take all orientations with equal probability, the general expression for scattering into the small-angle region is given by

$$I(q) = [V_p(N_m b_m - N_o b_o)F(q)]^2. \quad (7)$$

It is constructive to examine the limiting values of the expression for $F(q)^2$, given by equation (4). To find an expression as $qR \to 0$, the following expansions are used:

$$\sin x = x - x^3/3! + x^5/5! - \ldots$$

and

$$\cos x = 1 - x^2/2! + x^4/4! - \ldots .$$

Then $F(q)^2 \to \exp(-x^2/5)$. The radius of gyration, $R_g$, of a sphere of radius $R$ is given by $R_g^2 = (3/5)R^2$; hence $F(q)^2 \to \exp(-qR_g^2/3)$, which is the expression given by Guinier (see Guinier & Fournet, 1955).

For the limit $qR \to \infty$, the trigonometrical terms are replaced by their averages over one cycle. These averages are $\langle \sin^2 x\rangle = 1/2, \langle \cos^2 x\rangle = 1/2, \langle \sin x \cos x\rangle = 0$. Then $F(q)^2 = 9/2(qR)^4$ and $I(q) = 2\pi(Nb)^2 S/q^4$, where $S$ is the surface area of the sphere. This limiting value is the origin of what is called ''Porod's law'', which is often incorrectly taken to imply that the scattering at large $q$ is dependent only on the surface area of the particle. The appearance of $S$ in the intensity expression is a consequence of the way in which the limit is taken and does not reflect the diffraction physics of the process. The scattered intensity is always proportional to the number of nuclei in the particle.

Calculations of the form factor for particles of shapes other than spherical have been made (Guinier & Fournet, 1955). For a rod of length $2R$ and negligible cross-section area,

$$F(q)^2 = [\mathcal{S}(2qR)/qR] - [\sin^2(qR)/(qR)^2], \quad (8)$$

where

$$\mathcal{S}(x) = \int_0^x \sin(t)/t\, dt.$$

For a disc of radius $R$ and negligible thickness,

$$F(q)^2 = [2/(qR)^2][1 - J_1(2qR)/qR]. \quad (9)$$

## 4. The profile function

The profiles predicted by equations (4), (8) and (9) oscillate because of the trigonometric terms. These oscillations will be seen in an experiment only if all the particles have the same shape and size to within a few percent. This is not often the case and a monotonic function, which has the same limiting values, is much more useful in the analysis of experimental data. Similar reasoning was used by Zachariasen (1945) in a discussion of dynamical X-ray diffraction by thick crystals in the Laue case.

It is proposed that small-angle scattering data can be analysed by the expansion of $I(q)$ in powers of the variable $\chi_j$, where

$$\chi_j = 1/[1 + (qR_j)^2/3]^{1/2}. \quad (10)$$

$R_j$ is a parameter with the dimensions of length specifying an average size or correlation length in the scattering object.

In the Guinier region ($q \to 0$), $\chi_j \to \exp(-q^2R_j^2/6)$, while in the Porod region ($q \to \infty$), $\chi_j \to 3^{1/2}/(qR_j)$.

In Fig. 1 it is shown that integral powers of $\chi_j$ reproduce the envelope of the classical solutions for the sphere, the disc and the rod. The variation of $F(q)^2$ with $q$ is shown for the first, second and fourth powers of $\chi_j$. The exact solutions (the full lines) are calculated from equations (4), (6) and (7).

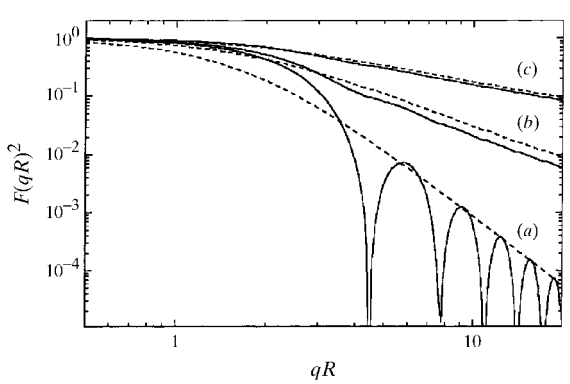


Fig. 1. A comparison of $\chi_j$, $\chi_j^2$ and $\chi_j^4$ [equation (10)] with the exact solutions for (*c*) the rod, (*b*) the disc and (*a*) the sphere. The exact solutions are the full lines.

There are other calculations of the scattering profile, as described in the following two sections.

### 4.1. *The 'Swiss cheese' problem*

This is a classic problem. The model quoted by the authors of the original solution (Debye *et al.*, 1957) is 'a distribution of holes of random shape and size in a solid'. The solution, in the notation of this paper, for the equivalent of the form factor squared is

$$F(q)^2 = 1/[1 + (qa)^2]^2,$$

where $a$ is a correlation length which, in the words of the authors, 'measures the grain size in the medium'.

### 4.2. *The fractal solution*

It has become common in recent years to use a solution in which $F(q)^2$ may be proportional to non-integral powers of $q$. Using the relations

$$\sin(\arctan x) = x/(1 + x^2)^{1/2}$$

and

$$\cos(\arctan x) = 1/(1 + x^2)^{1/2},$$

it can be shown that the fractal solution for $F(q)^2$ (Sinha *et al.*, 1984),

$$F(q)^2 = \frac{\sin[(D-1)\arctan(q\xi)]}{(1+q^2\xi^2)^{(D-1)/2}(D-1)q\xi}, \qquad (11)$$

reduces exactly to the formulae given in this work for values of $D = 2$ and $D = 3$. The quantity $\xi$ is the correlation length giving the size of the fractal structure.

For any non-integral value of $D$ between 2 and 3, it is possible to find a value $D'$ such that the evaluation of the expression

$$F(q)^2 = [1 + (q\xi)^2]^{-(D'-1)} \qquad (12)$$

is very close to that of (11). Fig. 2 shows a comparison between equations (11) and (12) for $D = 2.5$ and $D' = 2.4$.

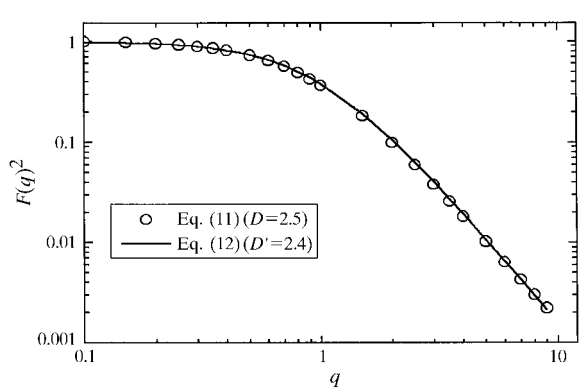


Fig. 2. Comparison of the fractal solution [equation (11)] with the solution predicted by equation (12) for $D = 2.5$ and $D' = 2.4$.

## 5. The intensity of multiple scattering

There are two cross sections relevant to the calculation of the extent of multiple scattering. The first is the total coherent cross section for scattering into the small-angle region by the particle, which, as noted by Halpern & Gerguoy (1949) and Dexter & Beeman (1949), is very much greater than the sum of the coherent cross sections of the nuclei in the particle.

To evaluate this term, the differential cross section per particle is written

$$d\Sigma/d\Omega = [V_p(N_m b_m - N_o b_o)]^2/[1 + (qR)^2/3]^2. \qquad (13)$$

The integral cross section per particle is found by integration over the solid angle of $4\pi$,

$$\Sigma = 3\lambda^2[V_p(N_m b_m - N_o b_o)]^2/4\pi R^2. \qquad (14)$$

The coherent cross section per unit volume for scattering into the small-angle region is then given by

$$\sigma = [\lambda(N_m b_m - N_o b_o)]^2 Rf \qquad (15)$$

where $f$ is the volume fraction of particles in the specimen.

The second, which is the cross section per unit volume for removal of neutrons from the small-angle region, is given by

$$\mu = f[N_m(\sigma_{sm} + \sigma_{am})] + (1 - f)[N_o(\sigma_{so} + \sigma_{ao})]. \qquad (16)$$

The total scattering cross section per molecule, including both coherent and incoherent scattering, is $\sigma_s$. The coherent component is the result of the first term in equation (3) or (6). In calculating the incoherent component, it is important to note that the true cross section will lie between the free-atom value and the bound-atom value. This is particularly important for molecules containing hydrogen. A detailed discussion is given by Lovesey (1984).

The total absorption cross section per molecule is $\sigma_a$, which is directly proportional to the neutron wavelength.

The total cross section per unit volume for removal of neutrons from the incident beam is $\tau$, which is given by $\tau = \sigma + \mu$.

## 6. The probability of multiple scattering

Let $N_n$ be the number of neutrons that have been scattered $n$ times. The number of neutrons incident on the specimen is $N$. In traversing a distance $\Delta t$ within the specimen, the number of neutrons scattered $n$ times is increased by the scattering into the small-angle region of those neutrons that have been previously scattered $(n - 1)$ times. The number of neutrons scattered $n$ times is decreased by further scattering into the small-angle region by scattering out of the small-angle region or by absorption. Then,

$$dN_n/dt = \sigma N_{n-1} - \tau N_n. \quad (17)$$

With the boundary conditions $N_o(0) = \Phi_0$, $N_n(0) = 0$, the solution of this equation is

$$N_n(t) = \Phi_0[(\sigma t)^n/n!]\exp(-\tau t). \quad (18)$$

The probability that a neutron has been scattered $n$ times in traversing a specimen of thickness $t$ is $N_n(t)/\Phi_0$.

The angular distribution of all neutrons after the beam has passed through the target is the probability-weighted sum of the individual angular distributions $P_n(q)$:

$$I(q) = \Phi_0 \exp(-\tau t)\sum_{n=1}^{\infty}[(\sigma t)^n/n!]P_n(q), \quad (19)$$

where each $P_n$ is normalized such that

$$(\lambda/2\pi)^2 2\pi \int_0^{4\pi/\lambda} qP_n(q)\,dq = 1. \quad (20)$$

Normalization ensures that the integrated intensity of each component in the profile is unity.

### 7. Multiple scattering and the profile function

Suppose that the angular distribution of neutrons elastically scattered $n$ times is $P_n(\mathbf{q})$. The probability of finding one of these neutrons in an element of solid angle $d\Omega$ in the direction $(\theta, \varphi)$ is $P_n(\mathbf{q})\,d\Omega$ with $d\Omega = \sin(\theta)\,d\theta\,d\varphi \approx (\lambda/2\pi)^2 q\,dq\,d\varphi$. After a subsequent collision, the momentum transfer of this neutron is $\mathbf{q}$ so that the angular distribution for neutrons scattered $(n+1)$ times is given by

$$P_{n+1}(\mathbf{q}) = \int P_n(\mathbf{q}_1)P_1(\mathbf{q} - \mathbf{q}_1)\,d\Omega_1. \quad (21)$$

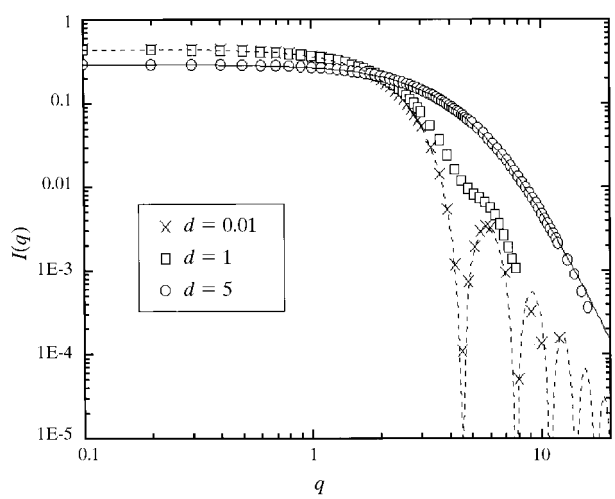


Fig. 3. The effect of self-convolution on the exact profile for the sphere. The cases shown are for sample thickness to neutron mean free path ratios ($d$) of 0.001, 1.0 and 5.0. The full line is the profile given by equation (27) with $p = 3$.

The distribution functions $P_n(\mathbf{q})$ are properly normalized angular distribution functions, $\int P_n(\mathbf{q})\,d\Omega = 1$.

The Fourier transform of $P_n$ is defined as $s_n(r) = \int \exp(i\mathbf{q}\cdot\mathbf{r})P_n(\mathbf{q})\,d\Omega$. If $P_n(\mathbf{q})$ depends only on the scattering angle $\theta$, this simplifies to

$$s_n(r) = (\lambda/2\pi)^2 2\pi \int J_0(qr)P_n(q)q\,dq, \quad (22)$$

where $J_0(qr)$ is the zeroth-order Bessel function.

Using the Faltung theorem for Fourier transforms, the transform of (21) becomes $s_{n+1}(r) = s_n(r)s_1(r)$, which leads to the general result

$$s_n(r) = [s_1(r)]^n. \quad (23)$$

The angular distribution of neutrons scattered $n$ times is then given by the inverse transform

$$P_n(q) = (2\pi/\lambda)^2(1/2\pi)\int_0^{\infty} J_0(qr)s(r)^n r\,dr. \quad (24)$$

To provide a simple demonstration of the effect of multiple scattering on the profile function, the Gaussian approximation is used. In this case,

$$P_1(q) = (2\pi/\lambda)^2(R^2/\pi)\exp(-R^2q^2) \quad (25)$$

and it is easily found that

$$P_n(q) = (2\pi/\lambda)^2(R^2/\pi n)\exp(-R^2q^2/n), \quad (26)$$

which shows that after $n$ collisions the observed width of the profile has increased by a factor of $n^{1/2}$.

A more interesting case is the profile function for identical spheres given by equation (4). The $n$-fold self-convolution of this function cannot be found analytically but can be derived by numerical methods. The results are shown in Fig. 3. The profile function rapidly approaches (as a function of $n$) the form given in equation (10) for $\chi_j$ raised to the sixth power.

When $P_1(q)$ is given by a profile function of the type given in equation (10),

$$P_1(q) = (I_0/\sigma)(1 + R^2q^2/3)^{-p}. \quad (27)$$

Determination of the inverse Fourier transforms cannot, in general, be carried out analytically. By numerical analysis it is found that $P_n(q)$ can be approximated closely by

$$P_n(q) = (I_0/\sigma n^{\alpha})(1 + R^2q^2/3n^{\alpha})^{-p} \quad (28)$$

after evaluation of the normalization factor in equation (20).

When $p = 3/2$, it can be shown that $\alpha = 2$. For other values of $p$, $\alpha$ can be approximated by an empirically determined function of $p$, obtained by least-squares fitting the results from the numerical evaluation of the inverse transform of $s(r)^n$ at different values of $n$ and $p$. A good approximation was found to be (see Fig. 4)

$$\alpha(p) = 1.48 + 2.37\exp[-3.17(p-1)], \quad (29)$$

$$I(q) = \Phi_0 \exp(-\tau t)(I_0/\sigma) \sum_{n=1}^{\infty} \{[(\sigma t)^n/n!n^\alpha] \times (1 + R^2q^2/3n^\alpha)^{-p}\}. \quad (30)$$

The intensity of the unscattered beam is

$$I_0(q) = \Phi_0 \exp(-\tau t) P_0(q),$$

where $P_0(q)$ is the angular profile of the incident beam normalized to an integrated intensity of unity. Thus the angular distribution of all neutrons after the beam has passed through the target is

$$I(q) = \Phi_0 \exp(-\tau t)\Big[P_0(q) + (I_0/\sigma) \sum_{n=1}^{\infty} \{[(\sigma t)^n/n!n^\alpha] \times (1 + R^2q^2/3n^\alpha)^{-p}\}\Big]. \quad (31)$$

Inspection of this equation shows, first, that term-by-term integration and summation of all terms leads to the expected result that the integrated intensity in the small-angle region is depleted only by the term $\exp(-\mu t)$. The same conclusion was reached by Dexter & Beeman (1949). Second, if the first term only under the summation sign is taken (single scattering), the kinematic differential scattering cross section of equation (13) is regained.

## 8. The total pattern

The total pattern is the sum of the scattered beam, the incident beam and the diffuse scattering, as follows.

### 8.1. *The scattered beam*

The scattered beam into the small-angle region is given by

$$I(q) = \Phi_0 C_1 \exp(-\tau t) \sum_{n=1}^{\infty} \{[(\sigma t)^n/n!n^\alpha] \times (1 + R^2q^2/3n^\alpha)^{-p}\}. \quad (32)$$

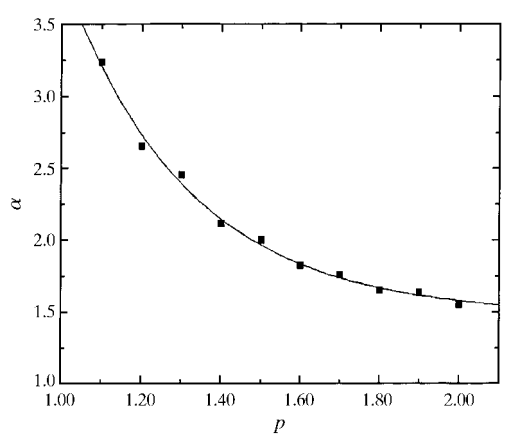


Fig. 4. Comparison of the empirical formula for $\alpha(p)$ with the points obtained by numerical analysis.

For spheroidal inhomogeneities, $C_1 = I_0/\sigma = 4\pi R^2/3\lambda^2$.

### 8.2. *The incident beam*

The incident beam is given, for a Gaussian incident-beam profile, by

$$I_0(q) = \Phi_0 C_0 \exp(-\tau t) \exp[-(bq)^2].$$

In this equation, $C_0 = 4\pi b^2/\lambda^2$ and, in terms of the full width at half-maximum ($q_w$) of the incident beam on the $q$ scale, $b = 2(\ln 2)^{1/2}/q_w$.

### 8.3. *The diffuse scattering*

The diffuse scattering for amorphous systems (both particles and matrix) is given by

$$I_d(q) = C_d \mu_s t,$$

where $C_d = \lambda^2/8\pi^2$.

## 9. An example of the use of the multiple-scattering method

The methods given in this work have been used to analyse experimental data for hydrated cement paste collected on the ultra-high-resolution SANS double-crystal diffractometer at Oak Ridge National Laboratory (Agamalian *et al.*, 1997). Since these experiments represent the commencement of a detailed analysis of SANS from hydrated and deuterated cement paste, no conclusions concerning the structure of cement will be made in the present work.

SANS profiles from cement paste samples of different thicknesses are shown in Fig. 5. In these measurements, the transmitted (unscattered) beam is sufficiently narrow for its contribution to the measured SANS profile to be ignored.

With any particular value of $\sigma$, fitting equation (32) to each SANS profile separately results in values $R_i(\sigma)$ and $A_i(\sigma)$ of the parameters $R$ and $A$, the latter being defined by $A = \Phi_0 C_1 \exp(-\tau t)$ for each sample thick-

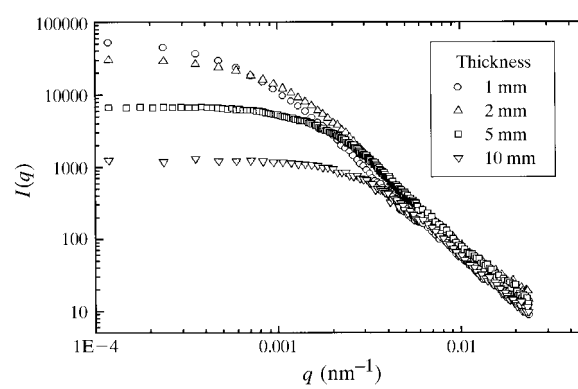


Fig. 5. SANS profiles obtained from four thicknesses of fully hydrated OPC cement.

ness $t_i$. Denoting the average value of the $R_i$ values by $\bar{R}(\sigma)$, the correct value for $\sigma$ is the value that minimizes the quantity

$$\chi^2 = \sum_i [\bar{R}(\sigma) - R_i(\sigma)]^2 \qquad (33)$$

so that the correct fitted $R$ value is $R = \bar{R}(\sigma)$. The results, shown in Fig. 6, yield values $\sigma = 1.08\ \text{mm}^{-1}$ and $\bar{R} = 1990$ nm.

The value of $\tau$ can then be obtained from the corresponding values $A_i$ by using the relation $\log(A_i/\Phi_0 C_1) = -\tau t_i$, plotting $\log(A_i/C_1)$ against $t_i$ as shown in Fig. 7. The points can be fitted with a straight line, the slope of which is the value of $\tau = 1.2$.

To estimate the errors on these parameters, the calculations are repeated a number of times using values of $A_i$ and $R_i$ randomly chosen within their error intervals. This procedure yields $R = 1990\ (60)$ nm, $\sigma = 1.0\ (1)\ \text{mm}^{-1}$ and $\mu = 0.14\ (2)\ \text{mm}^{-1}$.

## 10. Time-of-flight SANS

In SANS experiments carried out at spallation neutron sources, it has become customary to bin the data in steps of **q**. Since area detectors are used and a wide spectrum of neutron wavelengths fall upon the specimen, the neutrons arriving at a given value of **q** have a wide energy spectrum. Because of the details of the experimental arrangement, the bins at low values of **q** will receive a relatively greater number of low-energy (long-wavelength) neutrons.

When the experimental arrangement is such that the single-scattering approximation holds, this bias is of no consequence since inspection of equation (31) shows that the term for which $n = 1$ is independent of the neutron wavelength. The subsequent terms contain powers of the quantity $\sigma$, which has a strong ($\lambda^2$) dependence on the neutron wavelength. The qualitative conclusion is that, while the high-$q$ data may show little effect of multiple scattering, an assumption that the low-$q$ data are similarly unaffected is not necessarily valid.

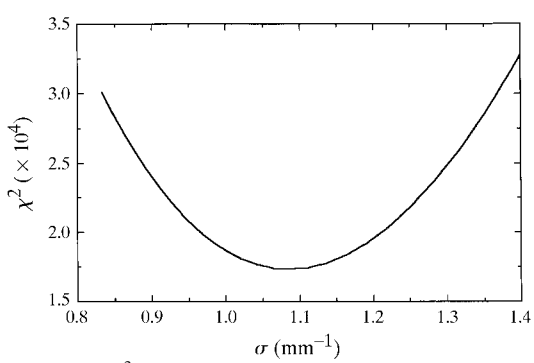


Fig. 6. A plot of $\chi^2$ *versus* $\sigma$ showing the strong minimum at $\sigma = 1.08$.

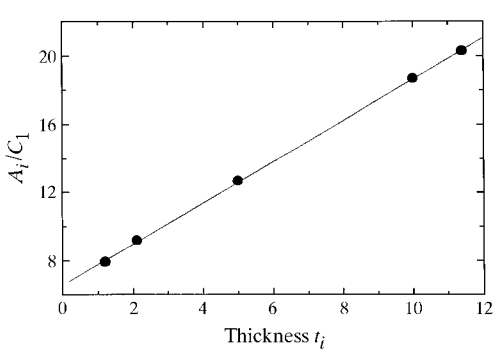


Fig. 7. A plot of the values $\log(A_i/C_1)$ *versus* sample thickness $t_i$. The slope of the fitted straight line gives a value of $\tau = 1.2$.

## 11. Conclusions

Use of the methods discussed in this work leads to an experimental design in which a number of different SANS profiles can be obtained from physically identical systems. As well as the well known technique of contrast variation (Jacrot, 1976), patterns can be obtained as a function of wavelength and of thickness. The situation becomes similar to that in conventional crystallography, in which many diffraction profiles contain different information about the values of the crystallographic parameters.

Refinement of the experimental profiles against the predictions of equation (31) will lead to values of $p$ (the shape of the object), $R$ (the size of the object), $\sigma$ (the absolute value of the SANS contrast) and $\mu$ (the chemical composition of the specimen).

We thank Dr L. P. Aldridge for his support and helpful discussions during the progress of this work.

### References

Agamalian, M., Wignall, G. D. & Triolo, R. (1997). *J. Appl. Cryst.* **30**, 345–352.

Cowley, J. M. (1981). *Diffraction Physics*, 2nd ed., p. 90. Amsterdam: North-Holland.

Debye, P., Anderson, H. R. & Brumberger, H. (1957). *J. Appl. Phys.* **28**, 679–683.

Dexter, D. L. & Beeman, W. W. (1949). *Phys. Rev.* **76**, 1782–1786.

Guinier, A. & Fournet, G. (1955). *Small-Angle Scattering of X-rays*. New York: John Wiley.

Halpern, O. & Gerguoy, E. (1949). *Phys. Rev.* **76**, 1117–1129.

Jacrot, B. (1976). *Rep. Prog. Phys.* **39**, 911–953.

James, R. W. (1948). *The Optical Principles of the Diffraction of X-rays*. Reprint (1982), pp. 465–467. Woodbridge, CT: Ox Bow Press.

Krivoglaz, M. A. (1969). *Theory of X-ray and Thermal Neutron Scattering by Real Crystals*, translated by S. C. Moss, pp. 130–132. New York: Plenum Press.

Lovesey, S. W. (1984). *Theory of Neutron Scattering from Condensed Matter*, Vol. 1, pp. 30–32. Oxford: Clarendon Press.

May, R. (1992). *International Tables for Crystallography*, Vol. C, edited by A. J. C. Wilson, pp. 105–112. Dordrecht: Kluwer Academic Publishers.
Mazumder, S. & Sequeira, A. (1989). *Phys. Rev. B*, **39**, 6370–6373.
Rietveld, H. M. (1969). *J. Appl. Cryst.* **2**, 65–71.
Sabine, T. M. (1992). *International Tables for Crystallography*, Vol. C, edited by A. J. C. Wilson, pp. 530–533. Dordrecht: Kluwer Academic Publishers.
Schelten, J. & Schmatz, W. (1980). *J. Appl. Cryst.* **13**, 385–390.
Sinha, S. K., Freltoft, Y. & Kjems, J. (1984). *Proceedings of the International Conference on Kinetics of Aggregation and Gelation*, edited by F. Family & D. Landau, pp. 87–90. Amsterdam: Elsevier.
Warren, B. E. (1949). *J. Appl. Phys.* **20**, 96–97.
Weiss, R. J. (1951). *Phys. Rev.* **83**, 379–389.
Zachariasen, W. H. (1945). *Theory of X-ray Diffraction in Crystals*. Reprinted (1967). New York: Dover.